

ENGINEERING-BASED TOOL FOR THREE-DIMENSIONAL ESTIMATIONS OF RE-ENTRY VEHICLES AEROTHERMODYNAMICS

Pasquale E. Di Nuzzo, Maria Maione, Giuseppe Pezzella & Antonio Viviani

Università della Campania "L. Vanvitelli", Dipartimento di Ingegneria. Via Roma 29, I-81031, Aversa (CE). Italy

Abstract

One of the most challenging aspects in designing a re-entry vehicle is the definition of its aerothermal loading environment. Indeed, due to high speeds involved, there's a significant increase in static temperature and pressure on the aeroshape surface, which can reach unsustainable levels. Therefore, an accurate estimation of thermal and mechanical limit loads is fundamental. Mapping convective heat flux over three-dimensional aeroshapes and identifying dangerous hotspots are essential for a safe vehicle design, especially during preliminary design phases and aeroshape optimization. A reliable estimation of surface heat fluxes helps to design a dependable thermal protection system made of suitable thermal protection materials. In this framework, the paper presents an engineering-based approach able to provide fast three-dimensional aerothermodynamic estimations for an assigned re-entry vehicle aeroshape. The reliability of these estimations is addressed by means of several result comparisons made with outcomes provided by more reliable accurate computational fluid dynamics investigations.

Keywords: lifting body, atmospheric re-entry, temperature, convective heat flux, surface streamline, TPS

1. Introduction

This research effort deals with an in-house developed engineering-based tool kit, namely HyHEAT, able to assess the convective heat transfer expected for generic re-entry bodies, such as capsules, lifting bodies, and winged vehicles for Low Earth Orbit (LEO) support servicing missions. HyHEAT, standing for Hypersonic Heat flux EstimAtion Toll, allows prompt evaluations of three-dimensional distributions of both convective heat flux and pressure expected for a spacecraft re-entering at hypersonic speeds, according to the trajectory-based design approach [1] [2] [3]. In this framework. the paper aims to apply and validate the HyHEAT tool to a Blended Wing Body (BWB) aeroshape, under development at the Department of Engineering of the University of Campania [4] [5] [6]. Tool reliability will be addressed by means of results comparison conducted between the outcomes of HyHEAT tool and those provided by more accurate Computational Fluid Dynamic (CFD) simulations. The evaluation will be made mainly under conservative turbulent flow conditions even though some assessments for laminar flow will be also provided for comparison aims. Air is assumed as an ideal gas since rather low hypersonic speed trajectory points were investigated so far (i.e., M_{∞} <10). HyHEAT relies on predictive models that, while less accurate than detailed simulations like CFD, are significantly faster. This makes the tool particularly suitable for feeding Multidisciplinary Design Optimization (MDO) procedures, which are fundamental to develop next-generation re-entry vehicles [7]. Indeed, HyHEAT is coded in Ansys Parametric Design Language (APDL) being a module of an in-house developed MDO procedure. Recall that MDO procedures are notably time consuming since they involve the investigation of thousands of aeroshape samples to provide the best one that satisfy all design requirements in the light of several constraints. Therefore, a good preliminary estimation of heat flux distribution is crucial for designing the spacecraft Thermal Protection System (TPS) and, then, selecting appropriate Thermal Protection Materials (TPM) throughout the whole design cycle of the spacecraft. The primary challenge faced by a spacecraft during re-entry is to withstand the extreme aeroheating due to the sudden conversion of its huge kinetic and potential energies in heat that takes place when the airflow crosses the strong bow shock wave in front of it.

2. Vehicle aeroshape

The spacecraft configuration investigated to prove HyHEAT reliability is the BWB aeroshape shown in Figure 1 [4] [5] [6].

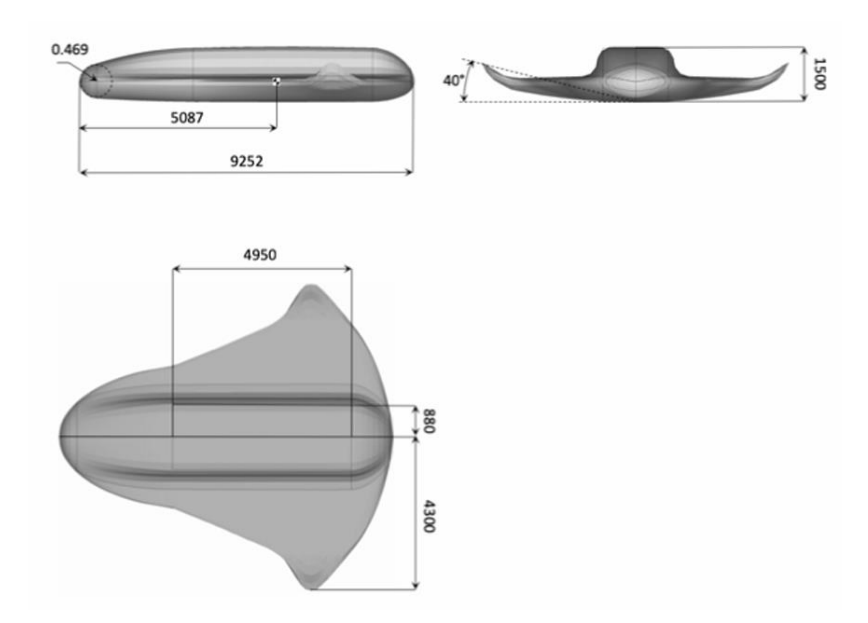


Figure 1- Three-views of BWB configuration adopted for aeroheating computations.

It is developed by authors by means of MDO procedures since the design of re-entry vehicles involves large number of design variables which usually result in conflicting trends [8]. As well known, in fact, a multi-disciplinary analysis relies on several design disciplines as, for instance, aeroshape definition, aerodynamic analysis, trajectory assessment, and aeroheating evaluation which are closely interconnected, as shown in Figure 2 where a part of the design structure matrix is provided.

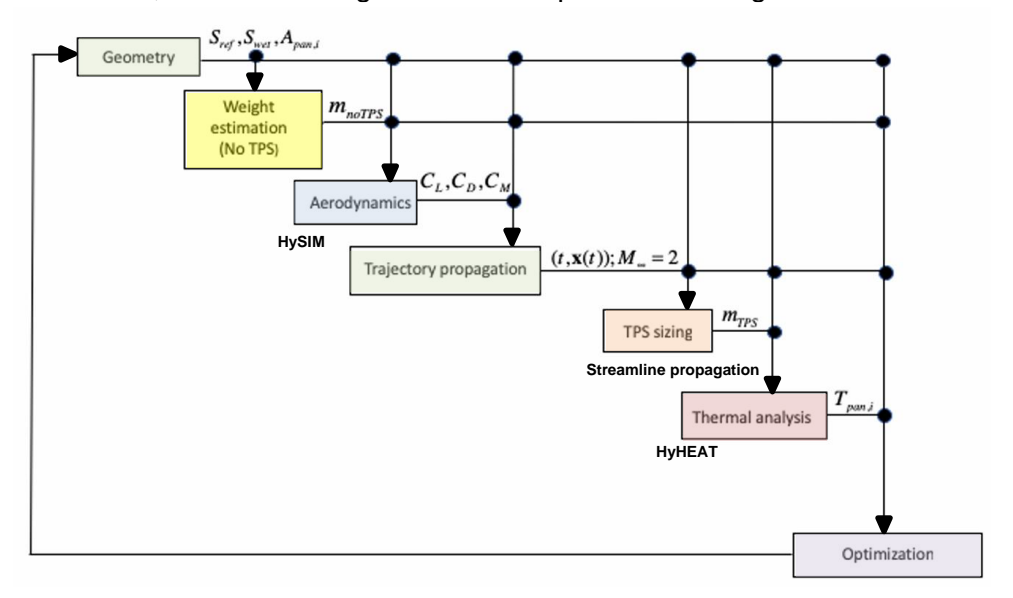


Figure 2-Multidisciplinary design structure matrix.

As well known, each sub-discipline analysis is performed independently and provides the input parameters for the next analysis. Sub-discipline models are finally connected to an optimization algorithm. A proprietary geometry module gives a support for several engineering-level methods which comprises: a multi-regime aerodynamic analysis (i.e., Hypersonic/Supersonic flow) performed with the HySIM panel method flow solver; a three degree of freedom non-planar trajectory estimation; a trajectory-based aeroheating analysis for aerothermal loading assessment, performed with

HyHEAT, and TPS sizing; and, at least, a mass estimation procedure [7] [8].

3. The HyHEAT aeroheating tool kit

3.1 State of the art of aeroheating tools

Most aerodynamic heating prediction tools rely on the Prandtl's boundary layer theory, starting with an inviscid solution of the velocity and pressure fields over the body surface to which a viscous correction is then applied [9]. The inviscid solution is often supplemented by engineering tools based on panel methods due to their computational efficiency in terms of run time calculation and accuracy of results. Techniques for boundary layer correction include splitting the vehicle into parts for analytical viscous solutions or using an axisymmetric analogy [10], which offers high accuracy but requires complex calculations of inviscid streamlines. DeJarnette and Hamilton's theory on inviscid streamlines, developed in Ref. [11] for the assessment of inviscid surface streamlines and heat transfer loading on shuttle-type configurations, is foundational. Hamilton et al. highlighted the strong influence of vehicle aeroshape on flowfield calculation methods [12]. In recent years, research engineers developed predictive engineering-based tools like AEROHEATING, INCHES, and AA3DBL [13]. Hamilton et al. created LATCH, but it's complex and not compatible with unstructured Euler solvers. Dyakonov and DeJarnette worked on applying axisymmetric analogy to surface grids made of triangular cells. DeJarnette et al. enhanced streamline metric calculation and developed UNLATCH2 and UNLATCH3, extending predictive capabilities [14]. The method involves splitting grids into parts with only two independent coordinates and integrating two coordinates along each streamline. Simplifying surface fitting equations and adapting approaches from Zhao et al. [15] and Parhizkar and Karimian were pursued for easier implementation [16].

3.2 HyHEAT overview

The formulation of heat fluxes is based on the resolution of the three-dimensional (3D) boundary layer using the axisymmetric analogy developed by Cooke, with corrections by Hamilton et al. and the Fay-Riddell formulation for stagnation points (i.e., for fuselage and wing/tail leading edges) [17]. This advanced theory inherently includes the Reynolds analogy, which relates the local skin friction coefficient to the heat transfer coefficient, thus allowing the estimation of a single streamline contribution to spacecraft aeroheating [18]. The tool can calculate laminar, transitional, and turbulent convective heat fluxes. Several engineering criteria for assessing turbulent transition are integrated into the tool and automatically applied in the calculations. The estimation of 3D surface heat flux begins with determining the wall streamlines, which are tracked onto the vehicle surface grid. The propagation of these streamlines is achieved through the numerical integration of 3D streamline equations using the second-order Runge-Kutta method [19]. Near the stagnation region of the body, the thermal formulation diverges from the axisymmetric analogy due to the singularity at the stagnation point. In particular, the body surface is divided into two parts, namely stagnation region and outside region. The former vehicle part is delimited by the stagnation region border, which is identified using a cell pressure coefficient criterion; along the border (referred to as the ϵ -curve), the implemented thermal formulation is detailed by Hamilton et al. On the internal cells of the stagnation region, convective heat fluxes are obtained by interpolating between the thermal flux values at the stagnation point and those along with the ϵ -curve. Further, the heat flux on the stagnation point cells, calculated using the Fay-Riddell formulation, is adjusted by a curvature factor [17]. This coefficient, determined through a second-order geometric ellipsoidal fitting, accounts for the local curvature of the grid faces to account for 3D effects.

Finally, the outside region is analyzed using the axisymmetric analogy. Currently, the HyHEAT tool can provide:

- full body streamline coverage, with one streamline for each grid cell.
- Newtonian aerodynamic estimation using an in-house developed tool, namely HySIM [6].
- perfect gas formulation for air.
- Parhizkar metric formulation, which estimates reciprocal convergence/divergence based on the minimum normal distance between two adjacent streamlines.
- convective heat flux formulation with both cold wall and radiative equilibrium wall boundary conditions.

Additionally, three different empirical hypersonic boundary layer transition criteria are available:

- 1. An immediate transition criterion based on the Reynolds number boundary layer momentum thickness of the face versus the Mach number boundary layer edge ratio of the face [20].
- 2. A smooth transition criterion, corrected by three different intervals that determine laminar, transitional, or turbulent flow, as referenced in Wuilbercq's work [21]. An additional option based on Bishop's surface roughness parameter correlation is implemented, with the formulation described in the Schneider's work [22].
- 3. Local streamline Reynolds number transition criteria developed by NASA, with detailed transition formulation and empirical coefficients reported in the work by Gond and Quinn [23].

4. Re-entry aerothermal loading environment

4.1 Re-entry trajectory and aerothermal loads assessment

The envelope of possible trajectories that a spacecraft can pursue, i.e., the set of trajectories that the vehicle can withstand from a thermal, structural, and aerodynamic perspectives, constitutes the so-called re-entry corridor. To define the re-entry corridor, it's necessary to specify the limitations that force the spacecraft to reach sustainable altitudes and velocities. All of this, in the altitude-velocity plane, translates into tracing curves representing these limits and identifying the area of the allowed flight, thus excluding what is referred to as *no flight zone*. These flight constraints are the equilibrium glide limit, the maximum heat flux limit, the normal load limit, and the maximum dynamic pressure limit. The mechanical loads are proportional to $\rho_{\infty}V_{\infty}^2$ (i.e., dynamic pressure), while thermal loads are more critical than mechanical ones because of the proportional factor is $\rho_{\infty}V_{\infty}^3$. The mathematical model for a re-entry flight simplifies the trajectory of an unpowered vehicle as a planar path over a non-rotating spherical Earth, treating the vehicle as a point mass. This approach involves analyzing the spacecraft's motion along with both the tangent and normal directions of the flight path. Notably, in this context, the entry angle γ is defined as positive for an ascending flight path. From this conceptual framework, the differential equations governing the spacecraft's motion read [4]:

$$\frac{dV}{dt} = \frac{D}{m} - g\sin\gamma\tag{2}$$

$$V\frac{d\gamma}{dt} = \frac{L}{m} - (g - \frac{V^2}{r})\cos\gamma \tag{3}$$

altitude (z) and down-range (s) equations are:

$$\frac{dz}{dt} = V \sin \gamma \tag{4}$$

$$\frac{ds}{dt} = \frac{R}{r}\cos\gamma\tag{5}$$

where:

$$L = \frac{1}{2} \rho_{\infty} v_{\infty}^2 S_{ref} C_L \tag{6}$$

$$D = \frac{1}{2} \rho_{\infty} v_{\infty}^2 S_{ref} C_D \tag{7}$$

$$g = g_0 \left(\frac{R}{r}\right)^2 \tag{8}$$

These motion equations need to be integrated, for this reason it's essential to define the atmospheric model to describe the variation of parameters with altitude and, specific initial (i.e., at the entry interface) conditions must be set. Initial conditions include the Mach number, M_{∞} , velocity, V_{∞} , reentry trajectory angle, γ_{∞} , entry altitude, H_{∞} , as well as the spacecraft aerodynamic database C_L and C_D (which depend on the angle of attack, α , and the flight Mach number, M_{∞}).

The re-entry trajectory foreseen for the BWB under investigation is provided in Figure 3, according to Ref. [4]. As shown, in this figure both the re-entry corridor and the guidance law $\alpha = \alpha(M_{\infty})$ are also shown.

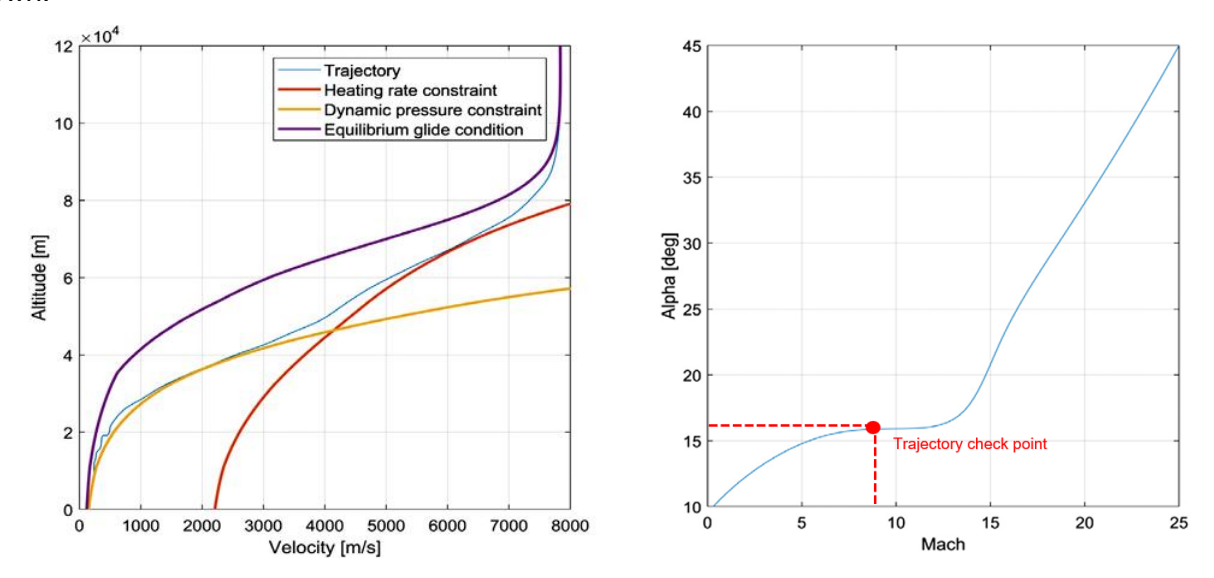


Figure 3-Spacecraft re-entry trajectory [4].

The re-entry corridor refers to the dynamic pressure limit Q_{max} =14 kPa, heat flux limit \dot{q}_{max} =600 kW/m² (vehicle nose radius R_N =0.469 m), and the equilibrium glide curve with C_{Lmx} =0.75 [4].

5. CFD and HyHEAT analysis

Once the re-entry trajectory is available, some check points (i.e., flight conditions) can be chosen to assess the aerothermal loads the BWB must withstand during descent, according to the trajectory-based design approach.

The trajectory check point chosen in this research effort is shown in Figure 3. Therefore, its free-stream conditions, provided in Table 1, are considered to carry out both CFD and engineering-based simulations to address the spacecraft aeroheating with radiation cooling at wall. Recall that, computations were performed for both laminar and fully turbulent flow conditions, as detailed discussed in the following paragraph 4.1 and 4.2. respectively.

Altitude, H_{∞} [m]	42.0×10^3
Sound speed, a_{∞} [m/s]	320.7
Mach number, M_{∞}	9.3
Angle of attack, α [deg]	16.0
Static Temperature, T_{∞} [K]	255.9
Dynamic viscosity, μ_{∞} [Pa s]	1.6293×10^{-5}
Adiabatic index, γ [-]	1.4 (perfect gas)

Table 1- Trajectory Check point.

5.1 CFD results

CFD simulations are performed with the ANSYS-FLUENT[©] tool on structured grids close to that shown in Figure 4. Here the mesh is provided on the vehicle surface and symmetry plane [24]. This grid, developed in ICEM-CFD [25], is made of 80 blocks for an overall number of about 6 M cells for the half body [26].

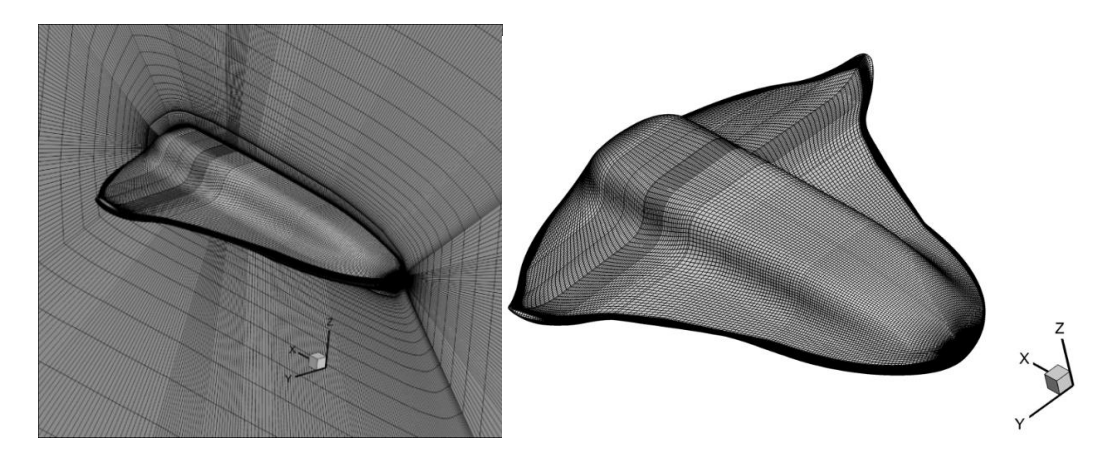


Figure 4- Structured mesh used in the CFD analysis [26].

The flowfield simulation relies on a density-based, implicit, second order, and fully turbulent approach, where the thermo-chemical effects are not taken in account due to the rather low free-stream Mach number, see Table 1. Therefore, the assumption of an ideal gas is made, but with seven degrees-of freedom activated to account for the molecular vibrational excitation. For the specific heat coefficient at constant pressure, c_p , a polynomial formulation with temperature has been considered. The numerical method chosen to solve the advection equation is the Advection Upstream Splitting Method (AUSM) one, which is especially effective for simulating compressible flows at hypersonic speed.

Finally, flow turbulence is addressed by means of the k-ω SST (Shear Stress Transport) model. Achieved numerical results in terms of temperature and pressure coefficient are provided hereinafter. For instance, the temperature distribution on the body surface is shown in Figure 5.

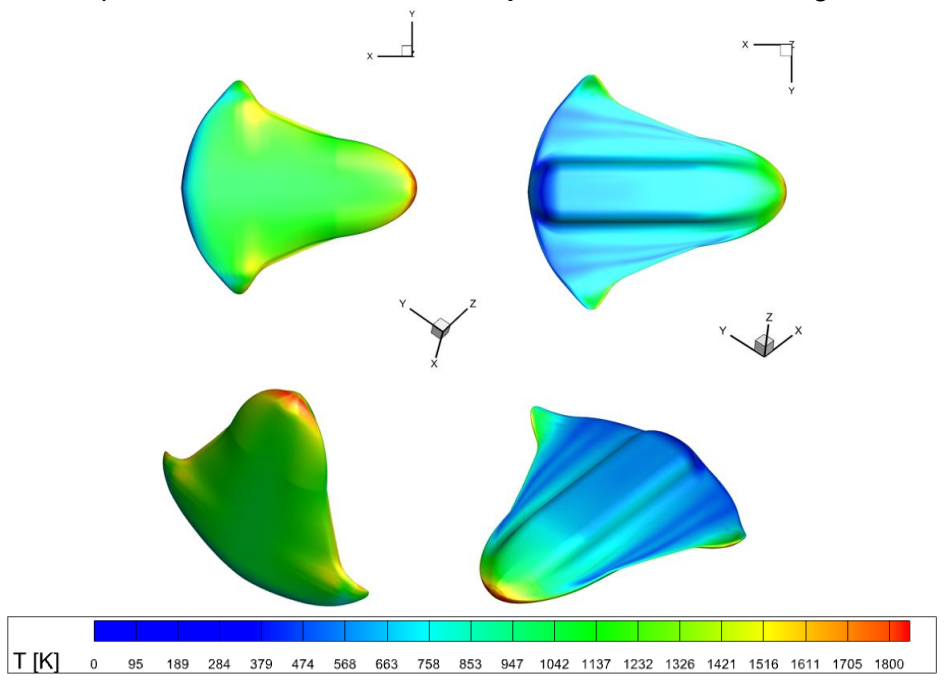


Figure 5-Temperature [K] contours for fully turbulent flow conditions. CFD results.

As expected, the highest temperatures are found on both fuselage and wing leading edges (i.e., stagnation regions) due to the local strong shock waves that occur in these regions at hypervelocity conditions. Elevated temperatures are also noted on the spacecraft windside due to the rather high AoA, α ; while lower aeroheating take place on the vehicle leeside due to the flow expansion in this flowfield region. As far as contours distribution of convective heat flux (\dot{q}_w) is concerned, it is worth to note that present flowfield simulations are carried out under the assumption of radiation cooling (i.e., the conductive heat flux inside the TPS is assumed negligible). Therefore, according to the

Stefan-Boltzmann, it follows that:

$$\dot{q}_w = \sigma \epsilon T_w^4 \tag{9}$$

where σ is the Stefan-Boltzmann constant, ϵ is the TPS emissivity, and T_w is the wall temperature. As a results, contours map of \dot{q}_w mirrors the one of temperature shown in Figure 5. Contours of pressure distribution are displayed in Figure 6.

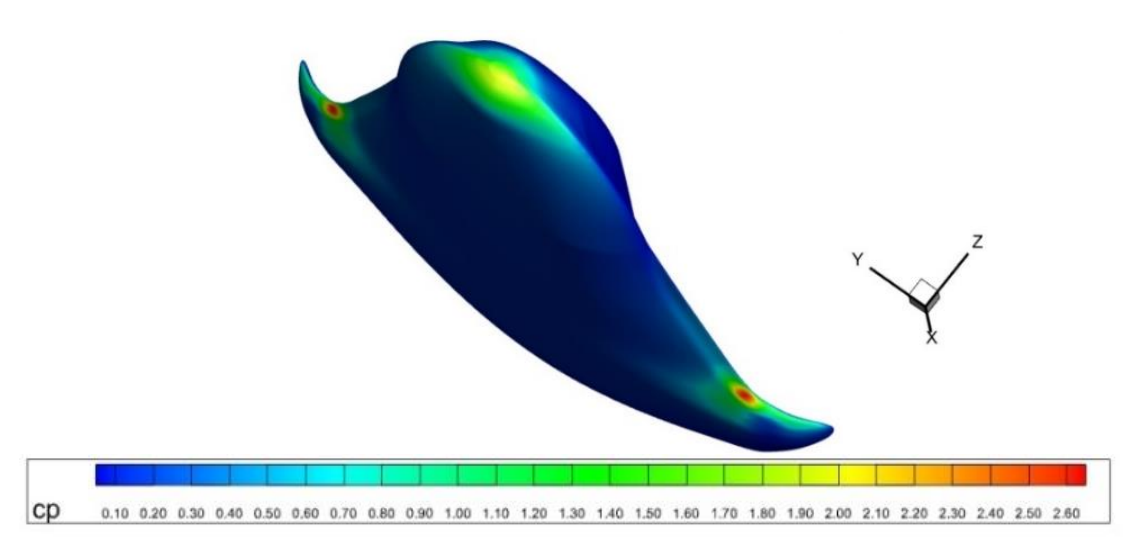


Figure 6-Pressure Coefficient contours in turbulent flow conditions. CFD results.

It's notable the value $c_p=1.8$ at the nose stagnation point, according to the modified Newtonian theory; while the pressure overshoot on the wing leading edge is due to the Shock-Shock Interaction (SSI) phenomenon that takes place between the spacecraft bow shoch and the one determined ahead of the wing. See Ref. [8] for more details.

5.2 HyHEAT results

Aeroheating investigations of HyHEAT were carried out on the surface mesh provided in Figure 7. It is an unstructured grid built with the ICEM-CFD tool [25].

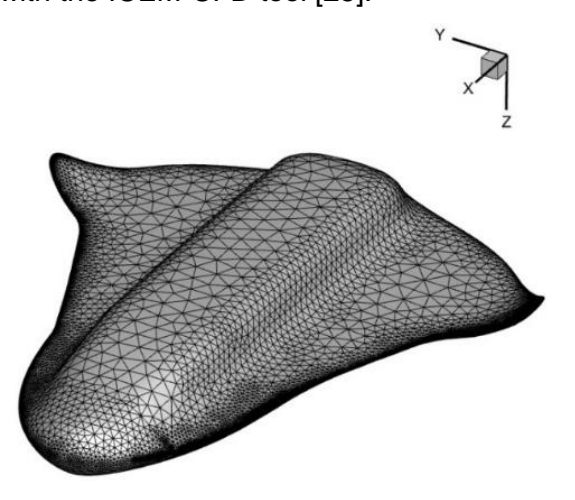


Figure 7- The unstructured surface mesh used in HyHEAT analysis.

Static temperature contours evaluated by HyHEAT are shown in Figure 8. As one sees, also HyHEAT results figure out that the highest temperatures are found on both the fuselage and wing leading edges, as expected. Recall that the heat flux at the stagnation point is proportional to the inverse of the square root of the local nose and wing leading edge radii.

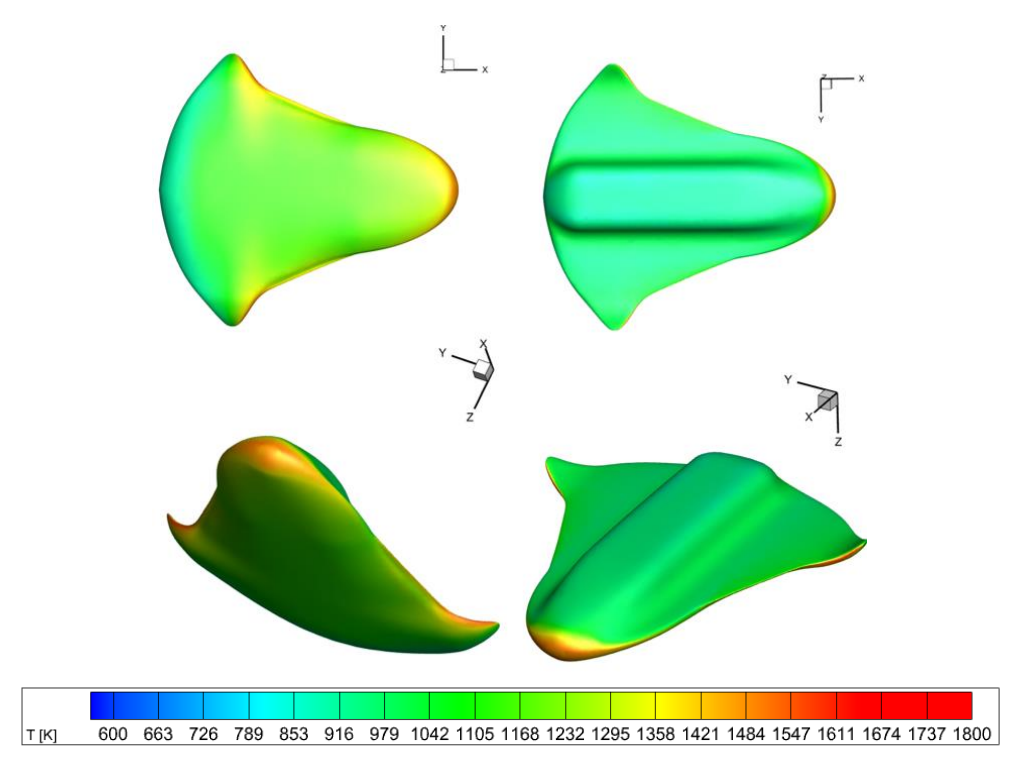


Figure 8-Temperature contours. HyHEAT results.

Further, the convective heat flux at nose is larger than the one on wing leading edge due to threedimensionality flow effects, say about 30%, even though the local geometric radius is the same [17]. In addition, at wing leading edge convective heat fluxes are mitigated by the effect of wing sweep angle, according the well know cosine law [27].

Finally, pressure contours are provided in Figure 9. Results point out that the maximum pressure is achieved at nose stagnation point. Recall that, the pressure overshoots highlighted by CFD on wing leading edges (see Figure 6) cannot be addressed by HyHEAT because of the tool is not able to account for SSI phenomena, as expected.

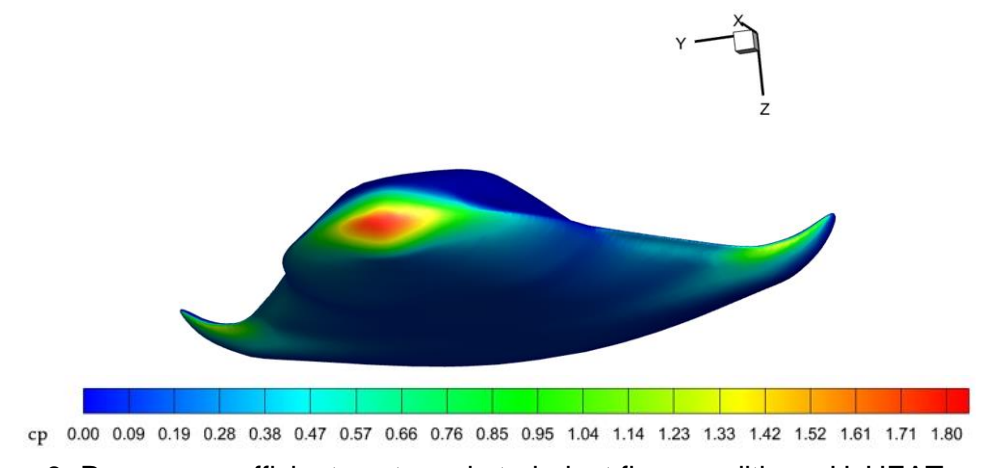


Figure 9- Pressure coefficient contours in turbulent flow conditions. HyHEAT results.

5.3 Comparison between CFD and HyHEAT results

Comparison between CFD and HyHEAT results are provided for both fully turbulent and laminar flow conditions by means of contours maps and diagrams. In particular, result comparisons by diagrams are provided considering the aeroshape curve sections provided in Figure 10, namely aeroshape centerline (i.e., y=0m) and cross sections $x_0=0.25m$, $x_1=2.39m$, $x_2=4.63m$, and $x_3=6.33m$.

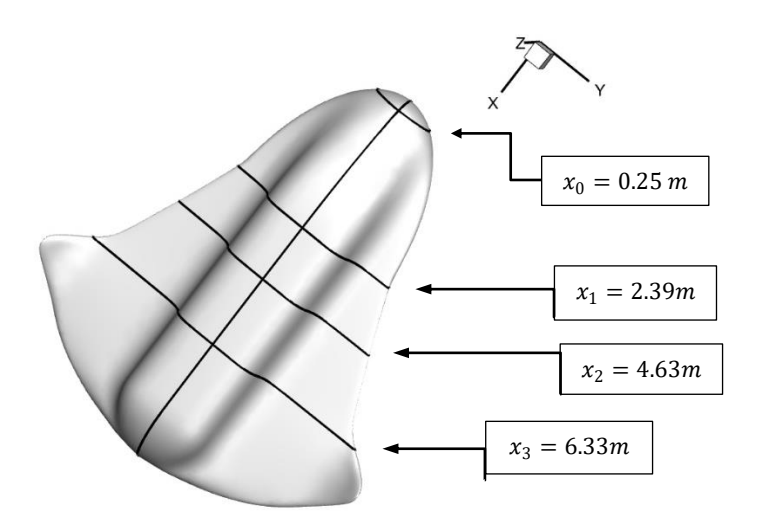


Figure 10- Centerline and cross-sections of the BWB aeroshape.

5.3.1 Turbulent flow conditions

Figure 11 provides contours map of temperature and pressure coefficient generated by juxtaposing two halves of the vehicle aeroshape. Specifically, on the left half of the aeroshape, the contours obtained from the CFD simulation are displayed; while on the opposite (i.e., the right half), the ones provided by HyHEAT analysis are shown. This representation allows highlighting differences and/or similarities between the results obtained with the two different approaches.

Results comparison in Figure 11 point out that low-fidelity HyHEAT outcomes compare rather well with those provided by more reliable CFD investigations. Further, a clear visualization of any discrepancies or correspondences between the two data sets is available, thus providing an immediate assessment of the accuracy and consistency of the engineering-based tool. This comparison suddenly helps identifying areas for improvement or confirmation in the HyHEAT models and calculations performed.

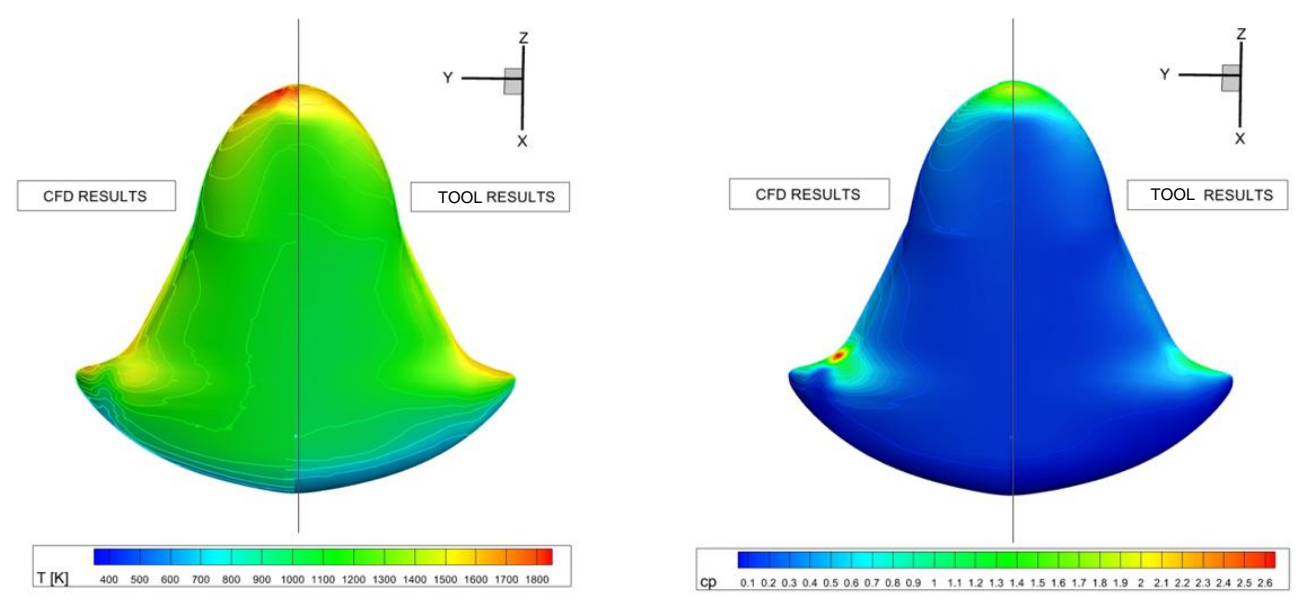


Figure 11- Comparison between CFD and HyHEAT result contours for temperature (left side) and pressure coefficient (right side).

As far as diagrams are concerned, Figure 12 highlights the results comparison along with the aeroshape centerline for both temperature (left side) and pressure (right side).

What is immediately noticeable is that HyHEAT and CFD results compare rather well each other even though some differences are clear at the spacecraft leeside.

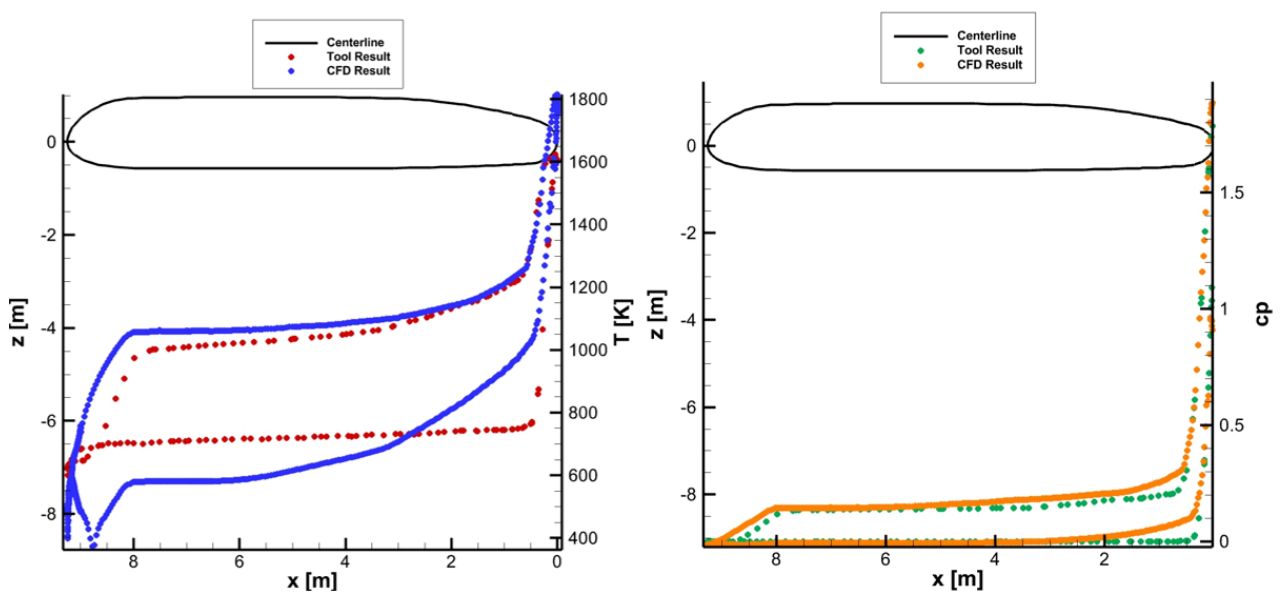


Figure 12- Results comparison along with the body centerline in turbulent flow condition for temperature and pressure coefficient, c_p.

Results comparison along with the body cross section x_0 =0.25m in turbulent flow conditions for static temperature and pressure coefficient, c_p , is summarized in Figure 13. HyHEAT outcomes are represented with dots, while CFD results with curves.

Temperature and pressure reach rather high values. For instance, at the aeroshape windside the static temperature is close to 1700K while pressure coefficient is larger than 1, as expected being the cross-section extremely close to the vehicle stagnation region.

As shown, HyHEAT once again seems capable of providing reliable design results, especially in the light of its very high simulation speed-up with respect to CFD.

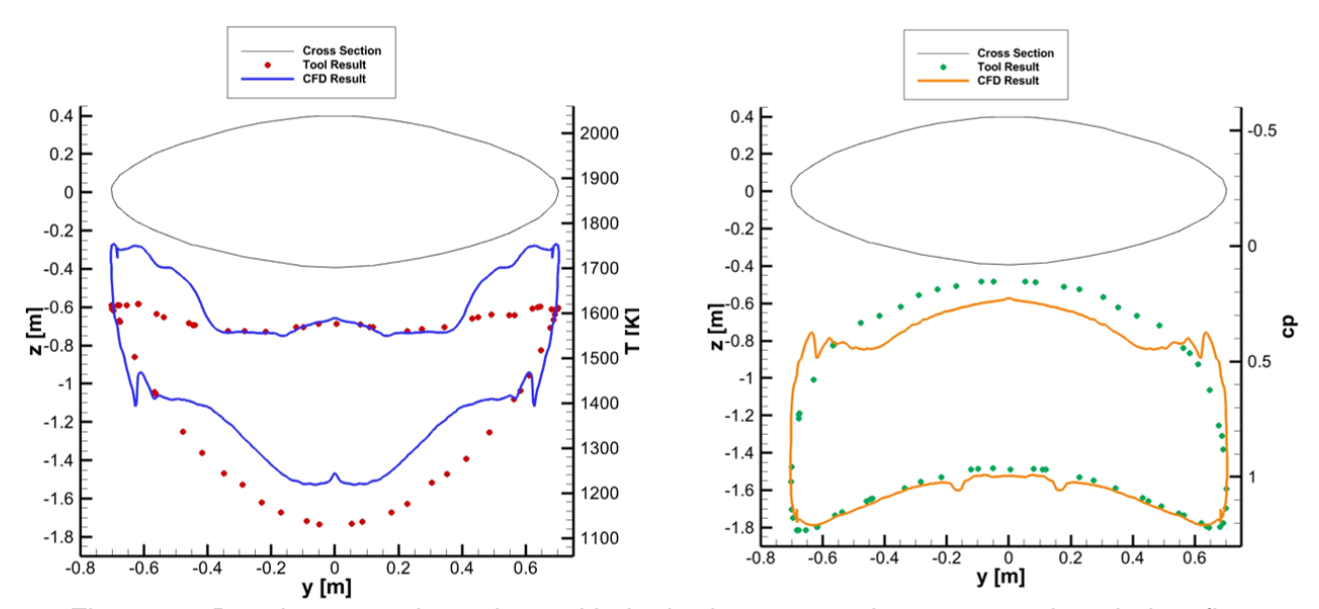


Figure 13- Results comparison along with the body cross section x_0 =0.25m in turbulent flow conditions for temperature and pressure coefficient, c_p .

The second cross-section being examined is the one at $x_1 = 2.39 \, m$. Result comparisons for temperature and pressure distributions at this cross-section are reported in Figure 14.

This figure points out that HyHEAT results compare rather well with CFD ones except at the leeside of wing strake leading edge, where local flow expansion is not captured well by the engineering-based tool.

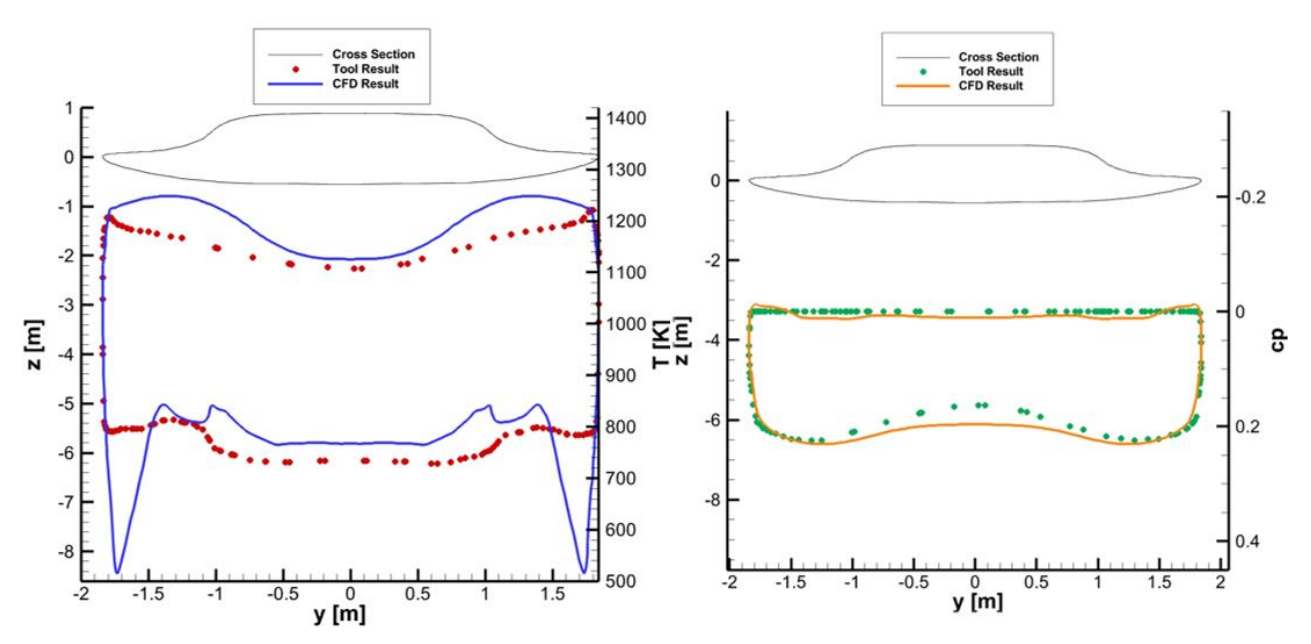


Figure 14- Results comparison along with the body cross section $x_1=2.39m$ in turbulent flow conditions for temperature and pressure coefficient, c_p .

Same result comparisons but for x_2 and x_3 cross sections are provided in Figure 15 and Figure 16, respectively. Once again, HyHEAT design investigations seem quite effective.

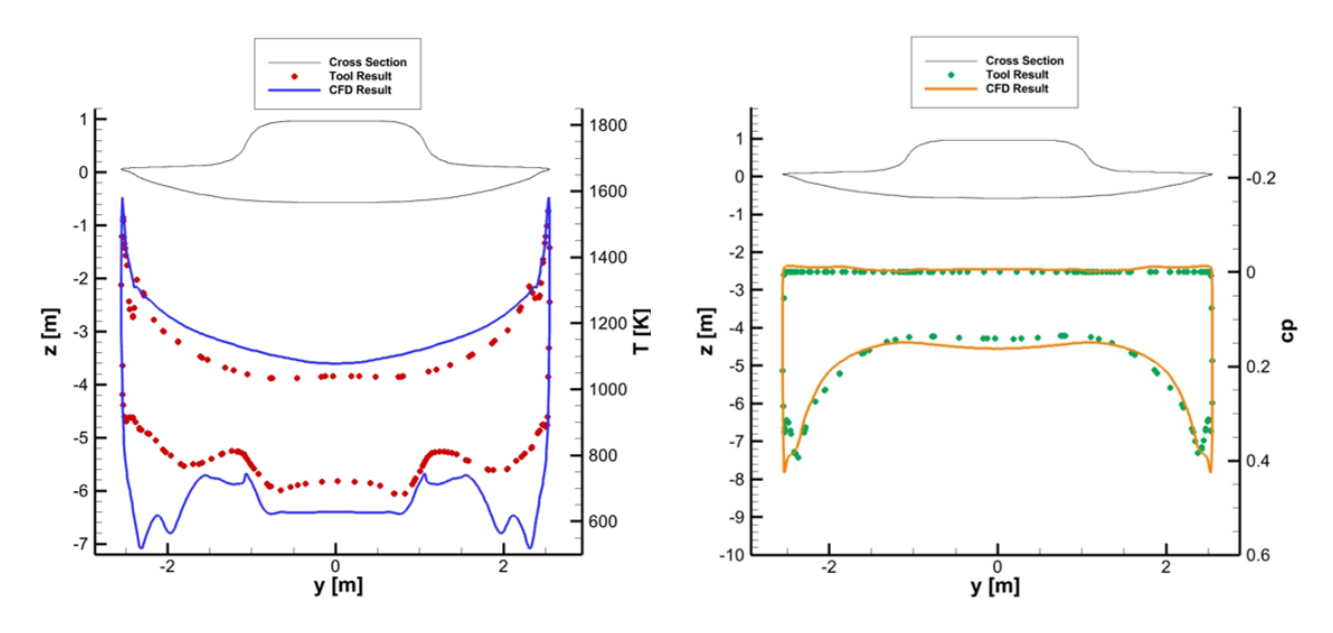


Figure 15- Results comparison along with the body cross section x_2 =4.63m in turbulent flow condition for temperature and pressure coefficient, c_p .

Anyway, moving away from the nose towards the spacecraft base, one would expect a reduction in temperature and pressure coefficient, which is indeed observed on both spacecraft leeside and windside. However, what stands also out when observing the temperature variation across these cross-sections is that the temperature undergoes a considerable increase moving towards the spacecraft wingtips. This is due to the local shape of the body, which is characterized by smaller

radii of curvature. Therefore, the increase of the temperature at the wing leading edges is related to its sharpness.

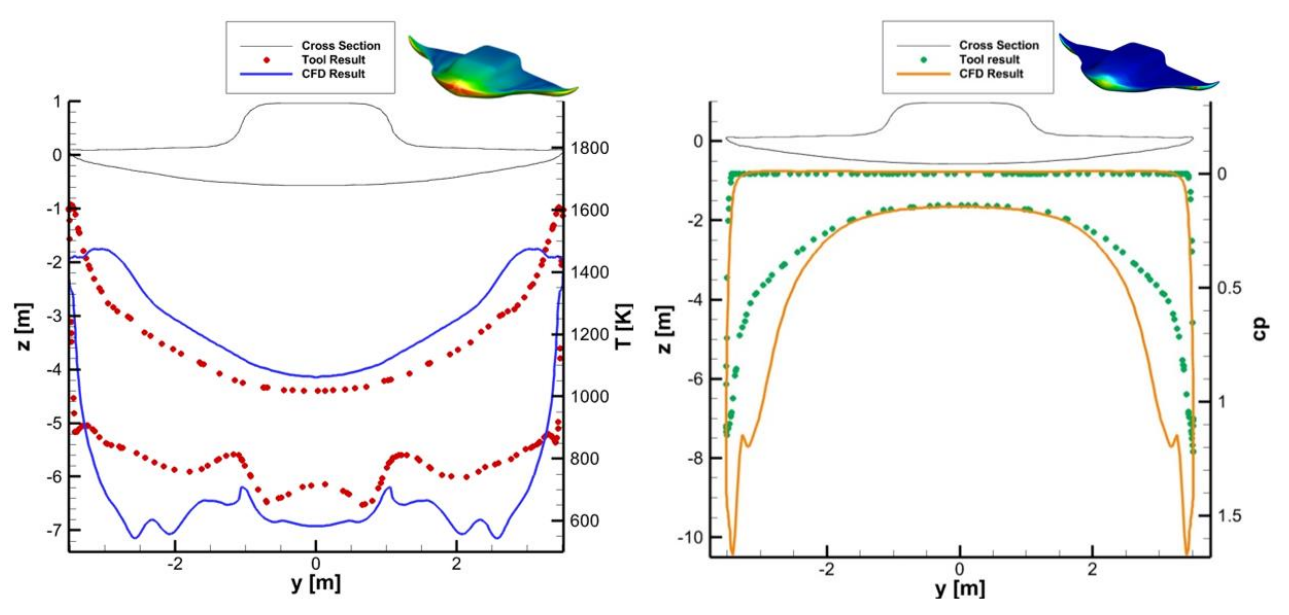


Figure 16- Results comparison along with the body cross section x_3 =6.33m in turbulent flow conditions for temperature and pressure coefficient, c_p .

Regarding the pressure coefficient, it has been noted that while the results from HyHEAT and the CFD simulations are quite comparable at the first three stations, at the fourth station, which includes the wing leading edge, the pressure coefficient trends tend to differ as one move along the wingspan. This phenomenon can be attributed to the fact that the CFD simulation is capable of accounting for the effect of SSI occurring near the wing leading edge. Such aerodynamic interaction can cause significant variations in the distribution of the pressure coefficient along with the wing, thus influencing the overall aerodynamic behavior of the configuration.

5.3.2 Laminar flow conditions

HyHEAT tool kit is also capable of simulating laminar flow conditions. For this reason, comparisons between its results and those from CFD are also included hereinafter. Nevertheless, only the result comparisons for temperature and pressure coefficient along with the aeroshape centerline and the x_3 cross section are presented for the sake of simplicity.

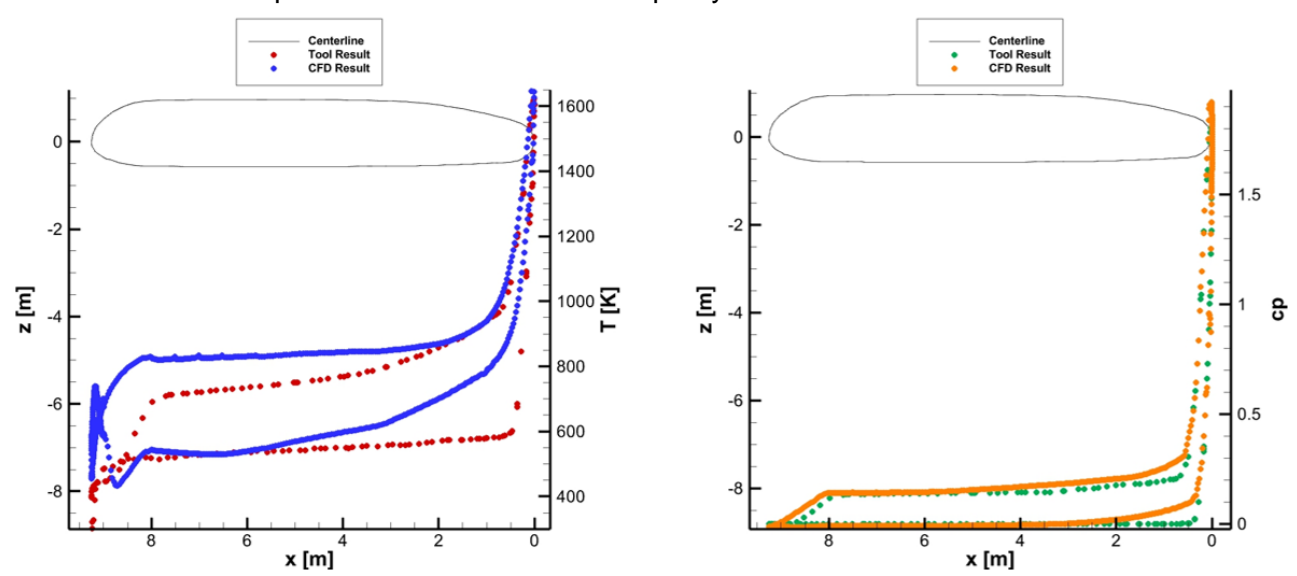


Figure 17- Results comparison along with the body centerline in laminar flow conditions for temperature and pressure coefficient, c_D.

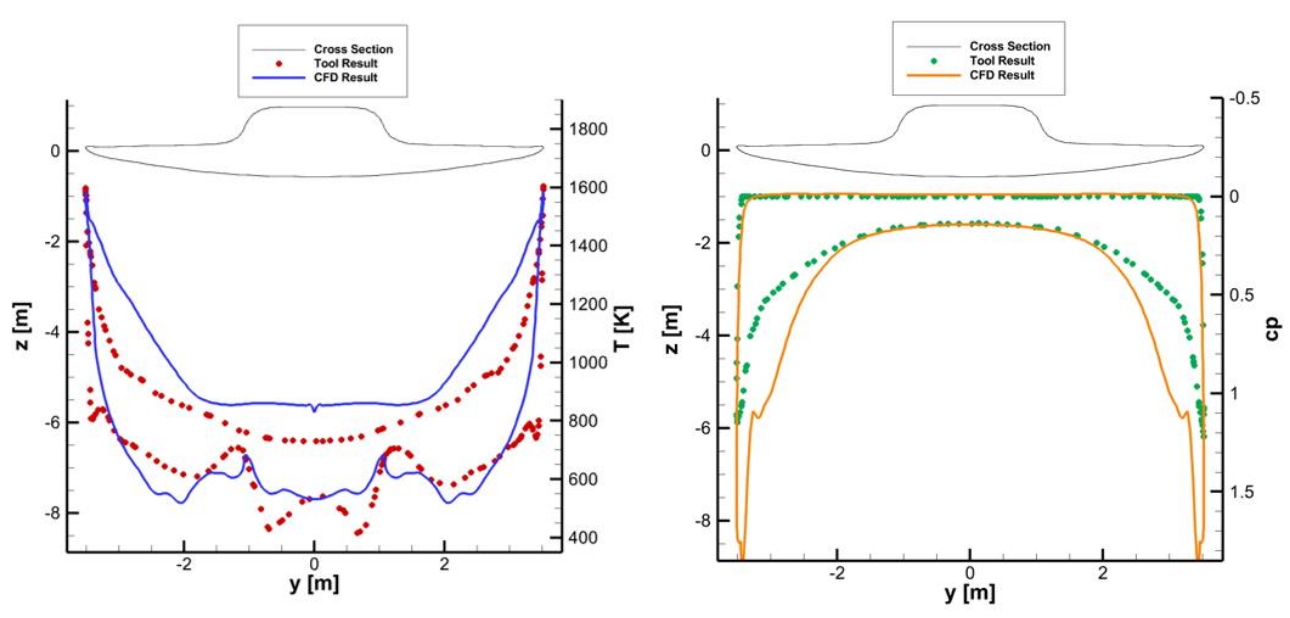


Figure 18- Results comparison along with the body cross section x_3 =6.33m in laminar flow conditions for temperature and pressure coefficient, c_p .

In laminar flow, the absence of intense flow mixing limits the heat transfer, thus maintaining an overall lower temperature compared to the turbulent case. No significant differences for the pressure distribution are detected passing from laminar to turbulent flow conditions, as expected.

6. Conclusions

The present paper dealt with a preliminary assessment of the reliability of an in-house developed engineering-based tool, namely HyHEAT. This tool kit is able to address the aerothermal loads expected during the descent flight for a space re-entry vehicle developed for low Earth orbit servicing. The validation was conducted by comparing the tool results with ones provided by more reliable numerical flowfield investigation for the same free-stream conditions and vehicle aeroshape. As seen from the result comparisons, HyHEAT and CFD outcomes compare quite well, but some discrepancies are possible when the focus in on local aeroshape parts interested by complex flowfield phenomena, such as shock-shock interaction and suddenly flow expansions not predictable by the engineering approach. Anyway, although HyHEAT may not capture all details and complex flow phenomena that CFD can predict, its performance is satisfactory, especially in the light of phase-A design, where prompt design results are mandatory for the aeroshape under investigation or optimization design procedures where thousands of samples must be processed.

7. Contact Author Email Address

mailto: giuseppe.pezzella@unicampania.it

8. Copyright Statement

The authors confirm that they, and/or their company or organization, hold copyright on all of the original material included in this paper. The authors also confirm that they have obtained permission, from the copyright holder of any third party material included in this paper, to publish it as part of their paper. The authors confirm that they give permission, or have obtained permission from the copyright holder of this paper, for the publication and distribution of this paper as part of the ICAS proceedings or as individual off-prints from the proceedings.

References

[1] D. K. Prabhu, "System Design Constraints – Trajectory Aerothermal," in *RTO AVT Lecture* Series on "Critical Technologies for Hypersonic Vehicle Development", von Kármán Institute, Rhode-St-Genèse, Belgium, 2004.

- [2] G. Pezzella, "Hypersonic environment assessment of the CIRA FTB-X re-entry vehicle," *Aerospace Science and Technology,* vol. 25, no. 1, pp. 190-202, 2013.
- [3] D. Kinney, "Aerothermal Anchoring of CBAERO Using High Fidelity CFD," in 45th AIAA Aerospace Sciences Meeting and Exhibit, Reno, Nevada. USA, 2007.
- [4] A. Aprovitola, N. Montella, L. Iuspa, G. Pezzella and A. Viviani, "An optimal heat-flux targeting procedure for LEO re-entry of reusable," *Aerospace Science and Technology,* vol. 112, p. 106608, 2021.
- [5] S. M. Giannino, G. Pezzella and A. Viviani, "Low Speed Aerodynamics of six optimised and unconventional re-entry vehicle aeroshapes," in *34th Congress of the International Council of the Aeronautical Sciences*, Florence, 2024.
- [6] N. Montella, G. Vio, L. Iuspa, A. Aprovitola,, G. Pezzella and A. Viviani, "Wind Tunnel Analysis of a Space Re-Entry Vehicle at Low-Speed Conditions," in *34th Congress of the International Council of the Aeronautical Sciences*, Florence, Italy, 2024.
- [7] L. Iuspa, A. Aprovitola, G. Pezzella, V. Cristillo and A. Viviani, "Multi-disciplinary optimization of a space re-entry vehicle using skeleton-based integral soft objects," *Aerospasce Science and Technology*, vol. 131, p. 107996, 2022.
- [8] A. Viviani, A. Aprovitola, L. Iuspa and G. Pezzella, "Aeroshape design of reusable re-entry vehicles by multidisciplinary optimization and computational fluid dynamics," *Aerospace Science and Technology*, vol. 105, 2020.
- [9] W. L. Hankey, Re-Entry Aerodynamics, Reston, VA. USA: American Institute of Aeronautics and Astronautics, 1988.
- [10] J. Cooke, «An axially symmetric analog for general three-dimensional boundary layers,» *Aeronaut. Res. Council Repts. Mem*, vol. 12, n. 3200, 1959.
- [11] F. R. De Jarnette and H. H. Hamilton, "Inviscid Surface Streamlines and Heat Transfer on Shuttle-Type Configurations," *Journal of Spacecraft and Rockets*, vol. 10, no. 5, pp. 314-321, 1973.
- [12] H. H. Hamilton, K. J. Weilmuenster and F. R. DeJarnette, "Approximate Method for Computing Convective Heating on Hypersonic Vehicles Using Unstructured Grids," *Journal of Spacecraft and Rockets*, vol. 51, no. 4, pp. 1288-1305, 2014.
- [13] E. V. Zoby, R. A. Thompson and K. E. Wurster, "Aeroheating Design Issues for Reusable Launch Vehicles -- A Perspective," in *34th AIAA Fluid Dynamics Conference*, Portland, Oregon, 2004.
- [14] H. Hamilton, J. Weilmuenster and F. DeJarnette, "Improved Approximate Method for Computing Convective Heating on Hypersonic Vehicles Using Unstructured Grids," in *9th AIAA/ASME Joint Thermophysics and Heat Transfer Conference*, San Francisco, California, 2006.
- [15] J. Zhao, L. Gu and H. Ma, "A rapid approach to convective aeroheating prediction of hypersonic vehicles," *Science China Technological Sciences*, vol. 56, no. 8, 2013.
- [16] P. a. Karimian, «Application of axisymmetric analog to unstructured grid for aeroheating prediction of hypersonic vehicles,» vol. 19, n. 3/4, 2008.
- [17] J. A. Fay and F. R. Riddell, "Theory of Stagnation Point Heat Transfer in Dissociated Air," *Journal of the Aerospace Sciences*, vol. 25, no. 2, pp. 73-85, 1958.
- [18] R. Wuilbercq, « Multi-Disciplinary Modelling of Future Space-Access Vehicles,» University of Stratclyde, 2015.
- [19] J. H. Ferziger, M. Perić and R. L. Street, Computational Methods for Fluid Dynamics, Springer, 2020.
- [20] S. K. Martinelli and R. D. Braun, "Centerline heating methodology for use in preliminary design studies," in *2011 Aerospace Conference*, 2010.
- [21] R. Wuilbercq, «Multi-Disciplinary Modelling of future Space-Access Vehicles,» 2010.
- [22] S. a. Lafayette, «Effects of Roughness on Hypersonic Boundary-Layer Transition,» *AIAA*, vol. 0305, n. https://engineering.purdue.edu/-aae519/BAM6QT-Mach-6-

ENGINEERING-BASED TOOL FOR ESTIMATIONS OF RE-ENTRY VEHICLES AEROTHERMODYNAMICS

- tunnel/reviewpapers/roughness-2007-0305.pdf, 2007.
- [23] Q. a. Gong, «Real-Time Aerodynamic Heating and Surface Temperature Calculations for Hypersonic Flight Simulation,» n. 4222, 1990.
- [24] «Ansys,» [Online]. Available: https://www.ansys.com/it-it/products/fluids/ansys-fluent.
- [25] «Ansys,» [Online]. Available: https://www.ansys.com/training-center/course-catalog/fluids/introduction-to-ansys-icem-cfd.
- [26] A. Viviani, A. Aprovitola, L. Iuspa and G. Pezzella, "Low speed longitudinal aerodynamics of a blended wing-body re-entry vehicle," *Aerospace Science and Technology*, vol. 107, p. 106303, 2020.
- [27] M. E. Tauber, "A review of high-speed, convective, heat-transfer computation methods," NTRS NASA Technical Reports Server, vol. 2914, 1989.
- [28] «Ansys,» [Online]. Available: https://www.ansys.com/it-it/partner-ecosystem/technology-partners/tecplot.